FISEVIER

Contents lists available at ScienceDirect

Earth and Planetary Science Letters

www.elsevier.com/locate/epsl



Origins of the terrestrial Hf-Nd mantle array: Evidence from a combined geodynamical-geochemical approach



Rosemary E. Jones ^{a,*}, Peter E. van Keken ^b, Erik H. Hauri ^b, Jonathan M. Tucker ^b, Jeffrey Vervoort ^c, Chris J. Ballentine ^a

- ^a Department of Earth Sciences, University of Oxford, South Parks Road, Oxford, OX1 3AN, UK
- ^b Department of Terrestrial Magnetism, Carnegie Institution for Science, 5241 Broad Branch Road NW, Washington DC 20015-1305, USA
- ^c School of the Environment, PO Box 642812, Washington State University, Pullman WA 99164-2812, USA

ARTICLE INFO

Article history: Received 3 October 2018 Received in revised form 18 March 2019 Accepted 9 April 2019 Available online 13 May 2019 Editor: M. Bickle

Keywords: mantle convection geodynamical modelling mantle geochemistry crustal evolution trace element partitioning

ABSTRACT

The formation and segregation of oceanic and continental crust from the mantle, and its return to the mantle via subduction and/or delamination, leads to the development of distinct geochemical reservoirs in the terrestrial mantle. Fundamental questions remain regarding the location, nature, and residence time of these reservoirs, as well as the respective roles of oceanic and continental crust in the development of the mantle's geochemical endmembers. The Lu-Hf and Sm-Nd isotope systems behave similarly in magmatic systems and together form the terrestrial mantle Hf-Nd isotopic array. Here we combine a geodynamic model of mantle convection with isotope and trace element (TE) geochemistry to investigate the evolution of the Hf-Nd mantle array. This study examines the sensitivity to: TE partition coefficients used in the formation of oceanic crust; density contrasts between subducting oceanic crust and the mantle; and the formation and recycling of continental crust. We show that the fractionation between the parent (Lu and Sm) and daughter (Hf and Nd) species needs to be higher than is indicated by partition coefficients determined from the present-day melting environment. This is consistent with the suggestion of deeper mantle melting earlier in Earth history and an increased role for residual garnet. Subduction and accumulation of dense oceanic crust produces a large mass of incompatible TE enriched material in the deep mantle. This deep mantle enrichment appears to play a more significant role than the extraction and recycling of continental crust in developing the Hf and Nd isotope and TE compositions of the mid-ocean ridge mantle source. The corollary of this result is that the formation of the continental crust plays a secondary role, contrary to the currently accepted paradigm. Nevertheless, the inclusion of continental crust formation and recycling produces a broader model mantle array, which better reproduces the spread in the natural data set. This model also produces the Hf and Nd isotope and TE compositions of the upper mantle and continental crust, as well as deep mantle compositions similar to those of plume-fed ocean island basalts. Our model is consistent with continental growth models based on the Lu-Hf isotopic composition of zircon, which suggest that 50-70% of the present-day mass of the continental crust is produced prior to 3 Ga, and that the recycling of continental crust becomes more prevalent after this time.

© 2019 Elsevier B.V. All rights reserved.

1. Introduction

The chemical and isotopic evolution of the terrestrial mantle is largely influenced by the formation of oceanic crust (OC) at spreading ridges and continental crust (CC) through arc volcanism, and the subsequent recycling of this crust back into the mantle via subduction and/or delamination. These processes produce the

* Corresponding author.

E-mail address: Rosie.Jones@earth.ox.ac.uk (R.E. Jones).

geochemical heterogeneity observed in samples such as ocean island basalts (OIB) and mid-ocean ridge basalts (MORB) that are derived from different parts of the mantle. The coupled Lu-Hf and Sm-Nd isotope systems have provided key insights into the evolution of the mantle and crust over the course of Earth history (Salters and White, 1998; Vervoort and Blichert-Toft, 1999; Vervoort et al., 1999; Chauvel et al., 2008). The mineral-melt compatibility of the radioactive parent isotopes (176 Lu and 147 Sm) is greater than their daughter species (176 Hf and 143 Nd, respectively) resulting in the residual mantle becoming more radiogenic than the extracted crust over time. The relatively long half-lives of these

systems (3.71×10^{10} yr for 176 Lu and 1.06×10^{11} yr for 147 Sm) compared to the age of the Earth, means that this isotopic divergence has been occurring over Earth history. Unlike U-Th-Pb, Lu-Hf and Sm-Nd are insensitive to redox conditions and relatively immobile in fluids, making these isotope systems ideal for investigating the dichotomy between the formation and recycling of oceanic and continental crust in driving the geochemical evolution of the mantle. In addition, the high concentrations of Hf in the mineral zircon allows for the combined measurement of Hf isotopic compositions and U-Pb ages (e.g., Kinny and Maas, 2003; Fisher et al., 2014; Jones et al., 2015; Vervoort and Kemp, 2016). This makes the Lu-Hf isotope system key to the development of models of continental crustal growth, preservation, and recycling (e.g., Hawkesworth and Kemp, 2006; Belousova et al., 2010; Condie et al., 2011; Dhuime et al., 2012).

There is strong evidence that recycled crust is present in the deep mantle and influences the source of plume-fed ocean islands (White, 2015 and references therein). OIBs have a wide range of isotopic compositions, which have been grouped into different categories (e.g., EMI, EMII, and HIMU White, 1985; Zindler and Hart, 1986; Stracke et al., 2005), 'Enriched' mantle (EM) endmember compositions are enriched in incompatible trace elements relative to MORB and are divided into two groups. EMI compositions have primarily been linked with the recycling of sediments (e.g., Weaver, 1991; Eisele et al., 2002), lower continental crust (Willbold and Stracke, 2006, 2010), or metasomatised subcontinental lithosphere (e.g., Zindler and Hart, 1986; Tatsumoto et al., 1992). EMII compositions have been attributed to the presence of small quantities of recycled terrigenous sediment (e.g., Zindler and Hart, 1986; Chauvel et al., 1992). HIMU OIBs are related to recycled oceanic crust, that has either had Pb preferentially removed by seafloor alteration and/or slab dehydration during subduction (e.g., Weaver, 1991; Chauvel et al., 1992; Peucker-Ehrenbrink et al., 1994; Kogiso et al., 1997) or has been enriched in U due to interaction with U-rich continental sediments after \sim 2 Ga (Elliott et al., 1999; Hanyu et al., 2014). The source of mid-ocean ridge basalts (MORB) is referred to as the depleted MORB mantle (DMM) reflecting its chemical depletion in incompatible TE as a result of upper mantle melting and crust formation.

Mass balance modelling is a useful way to investigate the geochemical evolution of the Earth. The resulting 'box models' provide some constraints on the relative interactions between reservoirs and the role of crust formation and recycling (e.g., Jacobsen and Wasserburg, 1979; Allègre and Lewin, 1995; Albarède, 1998; Coltice and Ricard, 1999; Kumari et al., 2016). Such studies can be further enhanced by full geodynamical modelling that can incorporate more realistic estimates on the rate of oceanic crust formation (which depends on plate velocities) and the subsequent remixing upon recycling (which depends on convective vigour), in turn controlled by the viscosity structure of the Earth's mantle. Christensen and Hofmann (1994) were the first to combine geodynamical modelling with geochemistry. They used a 2D Cartesian convection model to investigate the terrestrial U-Pb and Sm-Nd systems and found that extraction, recycling, and storage of oceanic crust in the deep mantle produced MORB-HIMU trends over 3.6 Byr. These early geophysical-geochemical model studies (see also Davies, 2002) imposed plate motions, and the recycling and remixing of oceanic crust were strongly influenced by these kinematic boundary conditions. Full dynamical models (e.g., Xie and Tackley, 2004; Brandenburg and van Keken, 2007) avoid the strong influence of external forcing through the boundary conditions and are more appropriate tools to study convective mixing in the Earth's mantle.

The combined geodynamical-geochemical model used in this study is based on an updated version of the model by Brandenburg et al. (2008). This mantle convection model uses a 2D cylindrical

geometry with a reduced core radius to better match the heat flow characteristics of the spherical Earth (van Keken, 2001). It incorporates plate tectonics through a force-balanced plate method, which causes plate movement in an energy-conservative manner. It reproduces some key physical features of plate tectonics and mantle convection including: a match to the present day heat flow and plate velocities (Brandenburg et al., 2008); sinking slab geometries that show similarities to mantle tomography (Van der Hilst et al., 1997; Ritsema et al., 2011; see van Keken, 2013 for a direct comparison); and accumulation of oceanic crust near the core-mantle boundary (CMB) (e.g., Spasojevic et al., 2010). The resulting models also satisfy key geochemical constraints with a more heterogeneous lower mantle preserved below a well-stirred upper mantle (Hofmann, 1997) and reproduce the observed geochemical distribution in multiple isotope systems (U-Th-Pb, Rb-Sr, Sm-Nd, and Re-Os) that define the DMM, HIMU, and EMI mantle endmembers (Brandenburg et al., 2008).

In this study, we extend this model to include the Lu-Hf isotope system and focus in particular on its co-evolution with Sm-Nd. During mantle melting, Hf and Nd are more incompatible than Lu and Sm and hence a greater proportion of these elements are partitioned into the melt and, therefore, to the newly generated crust. The Hf and Nd isotopic compositions are often expressed as epsilon (ε) values, where ε represents the deviation of the Hf and Nd isotope compositions (176Hf/177Hf and 143Nd/144Nd) of the material of interest relative to that of the chondritic reservoir (CHUR), measured in parts per ten thousand. The ε_{Hf} and ε_{Nd} compositions of OIB and MORB display a linear relationship, known as the mantle array (e.g., Vervoort et al., 1999) (Fig. 1). In this array the DMM shows positive $\varepsilon_{\rm Hf}$ and $\varepsilon_{\rm Nd}$ values and enriched mantle compositions (EMI, EMII) extend to negative ε_{Hf} and ε_{Nd} compositions. Average continental crust compositions are even more negative (upper CC: $\varepsilon_{\rm Hf} = -13.2 \pm 2.0$, and $\varepsilon_{\rm Nd} = -10.3 \pm 1.2$; Chauvel et al., 2014) and HIMU compositions lie slightly below the array with more negative ε_{Hf} relative to ε_{Nd} values (Fig. 1).

2. Geodynamical-geochemical model methods

Our models closely follow the modelling presented in Brandenburg et al. (2008). We use the same geodynamical models produced from finite element modelling. The geochemical modelling, which is performed as a post-processing step, is extended to investigate the Lu-Hf and Sm-Nd systems. We provide a brief description of our methods below and a more complete description in the Supplementary Information. A schematic representation is presented in Fig. 2.

We mimic the physical process of mid-oceanic ridge melting by batch melting of a small volume of mantle in the regions where plates diverge. In the geodynamical models we use this melting to separate a basaltic crust and harzburgitic residue from periditote. In the geochemical modelling we incorporate the effects of redistribution of isotope species during batch melting. In both cases we use the formulation of Christensen and Hofmann (1994) with an initial mantle composition of undepleted peridotite (bulk silicate earth (BSE) (McDonough and Sun, 1995)). We represent the peridotite lithology with two components that we call (following Christensen and Hofmann, 1994) 'eclogite' and 'harzburgite'. While recognising that the terms 'eclogite' and 'harzburgite' are mineralogical terms that are valid only in the upper mantle, we note that we do not model any phase changes in the mineral assemblages. As a consequence, we will, with apologies to the reader, refer to any tracer that melts to form OC as 'eclogite' and any tracer that is part of the residue during melting as 'harzburgite' irrespective of their position in the model. Upon melting the active eclogite tracers are physically repositioned at the surface to form new OC (Fig. 2). This approach allows us to dynamically investigate the role

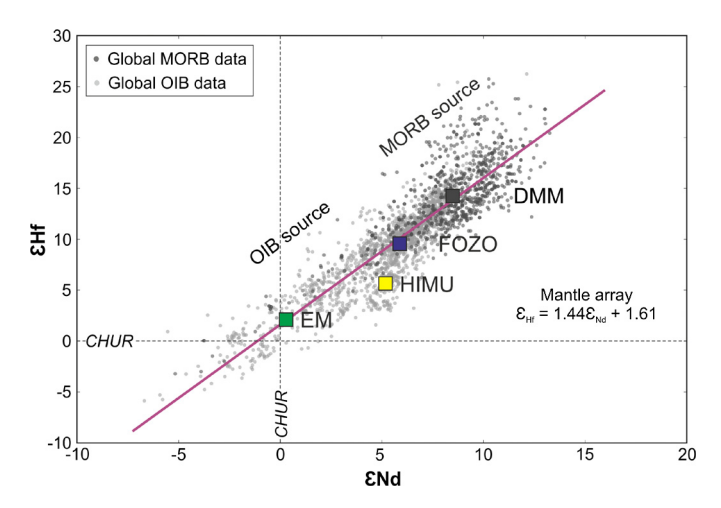


Fig. 1. ε_{Hf} and ε_{Nd} values for mid ocean ridge basalts (MORB) and ocean island basalts (OIB). The data were downloaded from the PetDB (www.earthchem.org/petdb) and GEOROC (http://georoc.mpch-mainz.gwdg.de/georoc/) databases in July 2017. The average compositions of the main mantle endmembers (DMM, FOZO, HIMU, EM) are shown by the large coloured squares, where EMI and EMII are treated as a single endmember due to their similar compositions in these isotope systems. The data used to calculate the average compositions were filtered as follows. DMM: all MORB data; HIMU: all St. Helena data (type locality), high $^{206}\text{Pb}/^{204}\text{Pb}$ (>20.0), and low $^{87}\text{Sr}/^{86}\text{Sr}$ (<0.7036); EM: all Kerguelen and Society data (EMI and EMII type localities) and high $^{87}\text{Sr}/^{86}\text{Sr}$ (>0.7045); FOZO: high $^{3}\text{He}/^{4}\text{He}$ (where R/R_a > 8) and low $^{87}\text{Sr}/^{86}\text{Sr}$ (<0.704). The ε_{Hf} and ε_{Nd} compositions of the upper continental crust (not shown) are -13.2 ± 2.0 , and -10.3 ± 1.2 respectively (Chauvel et al., 2014). The Hf-Nd mantle array follows the relationship $\varepsilon_{\text{Hf}} = 1.44\varepsilon_{\text{Nd}} + 1.61$; this is consistent with previously suggested relationships (e.g., Chauvel et al., 2008; Vervoort et al., 2011). (For interpretation of the colours in the figure(s), the reader is referred to the web version of this article.)

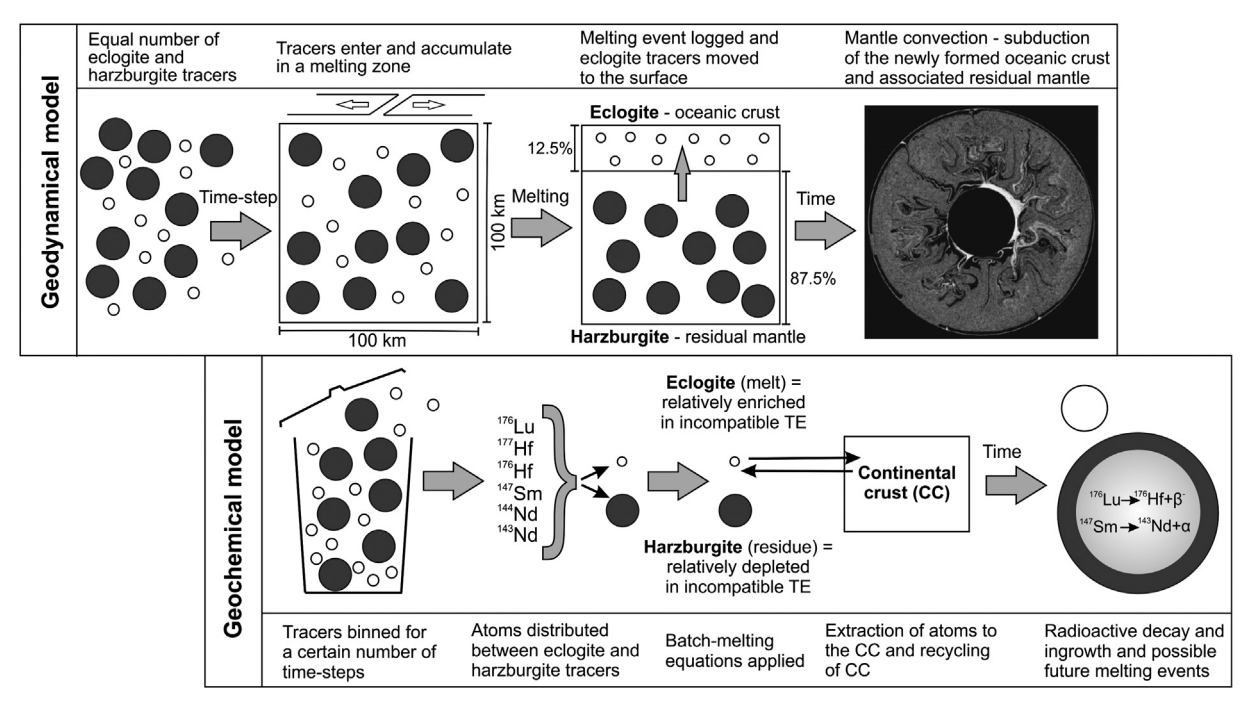


Fig. 2. A schematic of the geodynamical-geochemical model. In order to save on computational time, the geochemical modelling is run as a post-processing step where we access the logged melting information for each of the tracers in the geodynamical model output and compute the model chemistry based on melting events, radioactive decay/radiogenic ingrowth with time, and extraction and recycling of the continental crust.

of OC recycling on the dynamics of the mantle and its geochemical evolution. At depth, the OC is denser than the surrounding mantle by 3–7% in the upper mantle (Irifune, 1987; Ringwood, 1990; Aoki and Takahashi, 2004) and 0.5–5% in the lower mantle (Kesson et al., 1994; Hirose et al., 2005; Ono et al., 2005; Ricolleau et al., 2010). We use the geodynamical models of Brandenburg et al. (2008), which use a range of 0% to 10% of eclogite excess densities (EED), where an EED of 10% means that the eclogite tracers are 10% denser than the harzburgite tracers.

In the geochemical model, melting events are accumulated in 5 Myr intervals such that we have a sufficiently large number of tracers available for the batch melting calculations. We compute the total number of atoms of each isotope of interest by summing

the atoms present in the melt zone. We define a melt fraction (f) based on the relative volume of the combined eclogite tracers to total volume. This is a simple first-order parameterisation of melting at a mid-oceanic ridge where we will assume the melt fraction on average is 12.5% (e.g., McKenzie and Bickle, 1988). The eclogite tracers on average represent 12.5% of the mantle. During the model evolution the melt fraction varies around this fraction due to stochastic changes in the relative number of eclogite and harzburgite tracers for the EED = 0% case. For the cases with higher EED, an increasing number of eclogite tracers tend to remain in the deep lower mantle, and this reduces f by a few % over the course of the model run. We employ batch melting equations using the computed f and selected partition coefficients to find

the composition of the melt and residue. We then distribute the number of atoms in the melt equally between the eclogite tracers (thereby enriching them in incompatible elements) and distribute the atoms in the residue equally over the harzburgite tracers in the melt zone. We implement a number of published bulk D values in the model (Kelemen et al., 2003; Salters and Stracke, 2004; Workman and Hart, 2005), which are primarily derived from natural samples and selected in order to reflect large-scale global processes. Salters and Stracke (2004) present different Kd and mineral abundances for different pressures (2 and 3 GPa; representing depths of melting), resulting in large variations in the bulk D values produced for each element (Table 1).

In models where we simulate the formation of continental crust (CC), we further extract atoms from the recently melted eclogite tracers and store these in an extant CC reservoir. For this we use a separate set of partition coefficients. In Brandenburg et al. (2008) these were termed 'extraction coefficients' but, in an unfortunate error, the paper listed values for these coefficients that were actually the relative amount of atoms retained in the eclogite tracers, not that extracted to the CC. To be able to compare these coefficients with the previous paper we will list the relative amount retained as 'retention' coefficients. Newton iteration is used to determine the retention coefficients required to produce the present-day composition (Rudnick and Gao, 2014) and mass of the CC (2.4×10^{25} g) (CCpd).

In the preferred geochemical models of Brandenburg et al. (2008), two sets of retention coefficients were applied to fluidmobile elements (Pb, Th, Rb), before and after a somewhat arbitrary age of 2.25 Ga. This follows guidance from earlier box modelling (Rudge et al., 2005; Kellogg et al., 2007; and later by Kumari et al., 2016) and is required to provide a better fit between models and observations, in particular to Pb isotope data. As the trace elements considered here (Lu, Hf, Sm, Nd) are relatively immobile in fluids (Kessel et al., 2005), only one set of retention coefficients is applied. CC production starts at 4.0 Ga based on the age of the oldest continental crust (e.g., Bowring and Williams, 1999). The CC composition changes due to continued addition by CC extraction from the eclogite tracers and radiogenic ingrowth. We allow for the optional recycling of this evolving CC back into the mantle. potentially reflecting subduction erosion, delamination of the CC and/or the subduction of continentally derived sediments. When this functionality is applied, a fraction of the number of atoms of each isotope species (e.g., ¹⁷⁶Lu, ¹⁷⁶Hf, ¹⁷⁷Hf, ¹⁴⁷Sm, ¹⁴³Nd, ¹⁴⁴Nd), contained in the CC at a particular time interval, is removed and distributed to each eclogite tracer that has just participated in a melting event (i.e., newly formed OC).

3. Modelling approach and results

3.1. Approach

A step-wise approach was implemented to test the sensitivities of the Lu-Hf and Sm-Nd isotope systems to different variables and starting conditions, with increased complexity gradually built into the model. The aim of the modelling was to produce the composition of the present-day upper mantle (UM) ($\varepsilon_{\rm Hf} = \sim 14-18$ and $\varepsilon_{\rm Nd} = \sim 9-10$; White and Hofmann, 1982; Vervoort and Blichert-Toft, 1999; Chauvel and Blichert-Toft, 2001; Salters and Stracke, 2004; Workman and Hart, 2005), OIB endmembers, and CC (upper CC: $\varepsilon_{\rm Hf} = -13.2 \pm 2.0$, and $\varepsilon_{\rm Nd} = -10.3 \pm 1.2$; Chauvel et al., 2014), as well as the slope of the Hf-Nd mantle array (Fig. 1). The geochemical model parameters that remained constant are presented in Table 2.

3.2. Sensitivity to prescribed partition coefficients

We first tested the model sensitivity to different choices of partition coefficients (Fig. 3). The bulk D values of Workman and Hart (2005) produce a range of $\varepsilon_{\rm Hf}$ values that far exceed the range in the global dataset (+53 to -24 for EED = 10%, Fig. 3a). The bulk D values calculated using the mineral/melt partition coefficients (Kd) of Kelemen et al. (2003) and Salters and Stracke (2004) (for DMM at 2 GPa; Table 1) produce a much better fit to the global $\varepsilon_{\rm Hf}$ dataset (Fig. 3b and c). However, the opposite is the case for $\varepsilon_{\rm Nd}$, and in this case the bulk D values of Workman and Hart (2005) result in a better match (values ranging between +15 and -6, Fig. 3a), particularly in comparison to Salters and Stracke (2004) values for 2 GPa (Fig. 3c).

Kd values from Salters and Stracke (2004) for melting at 3 GPa produce a range of $\varepsilon_{\rm Hf}$ values that extend to much wider values than the global dataset (+59 to -47) and also result in the slope of the generated $\varepsilon_{\rm Hf}$ - $\varepsilon_{\rm Nd}$ array being far too steep (Fig. 3d). This is related to Lu being highly compatible in garnet (Table 1), which is present during mantle melting at higher pressures, resulting in a greater fractionation between Lu and Hf (i.e., $D_{\rm Lu}/D_{\rm Hf}$, Table 1), with less Lu being partitioned into the melt.

The published partition coefficients that best match the spread and slope of the Hf-Nd mantle array are those of Workman and Hart (2005) for Sm (0.045) and Nd (0.031) combined with those for DMM at 2 GPa (i.e., without garnet) from Salters and Stracke (2004) for Lu (0.137) and Hf (0.061) (Table 1, Fig. 3). A slight improvement on the fit can be achieved by adjusting the bulk D value for Hf to 0.066 (Fig. 3f). Bulk D values vary as a function of pressure and mineral abundance. As melting in the model extends to depths of 100 km, and as the mineral abundances in the mantle are likely to have changed over time, we consider adjusting the bulk D values within the range of those published (Table 1) to be realistic for the purposes of this large temporal and spatial scale modelling.

3.3. The effect of excess eclogite density (EED)

In the second stage of modelling we investigated the effect of changing EED on the geochemical evolution using the preferred bulk D values detailed above (Figs. 4, 5, and S1). In the neutral buoyancy case, the spread in Hf and Nd isotope compositions is more restricted than the global data array (Fig. 4a). There is also little variability in composition with depth and time (Fig. 4d) and the model is far from reproducing the $\varepsilon_{\rm Hf}$ and $\varepsilon_{\rm Nd}$ compositions of the UM, with average values of 1.0 and 0.7. As the EED increases the spread in the ε_{Hf} and ε_{Nd} values produced by the model also increases and more variability is observed with depth and time (Fig. 4). A notable feature is the development of increasingly unradiogenic Hf and Nd isotope compositions in the deep mantle. This reflects the accumulation of subducted eclogite at the CMB. The preferential partitioning of the daughter species (Hf and Nd) into eclogite results in the deeply stored OC developing less radiogenic compositions over time. With higher EED, more OC is stored at the CMB and more extreme negative $\varepsilon_{\mathrm{Hf}}$ and $\varepsilon_{\mathrm{Nd}}$ compositions develop (Figs. 4 and 5). The average $\varepsilon_{\rm Hf}$ and $\varepsilon_{\rm Nd}$ values in the deepest mantle in the EED = 10% model are -13.6 and -4.4. Conversely, the harzburgite tracers are relatively enriched in the parent isotopes (176Lu and 147Sm) and develop radiogenic Hf and Nd compositions over time. Areas of the mantle that contain a higher proportion of harzburgite compared to eclogite have positive $\varepsilon_{\rm Hf}$ and $\varepsilon_{\rm Nd}$, as is reflected in the composition of the UM (Figs. 4 and 5). The accumulation of eclogite tracers in the deep mantle is also demonstrated by the higher concentrations of incompatible TE near the CMB, which becomes more prevalent in the higher EED models (Figs. 5d-f).

 Table 1

 Published mineral/melt partition coefficients (Kd) and published/calculated bulk partition coefficients (bulk D) using different mineral modes. These are used and evaluated in the geodynamical-geochemical modelling.

Reference	Element	Mineral/m	elt partitio	n coefficien	ts (Kd)	Mineral mode	Bulk D values				D _{Sm} /	D _{Lu} /	(D _{Lu} /D _{Hf})/	Associated	
		Olivine Opx		Cpx Garnet		(refer to table below)	Sm Nd		Lu Hf		D _{Nd}	D_{Hf}	(D_{Sm}/D_{Nd})	figure	
Workman and Hart (2005)	-	-	-	-	-	Depleted MORB mantle (DMM)	0.045	0.031	0.120	0.035	1.45	3.43	2.36	Fig. 3a	
Salters and Stracke (2004) - 2 GPa	Sm Nd Lu Hf	0.0011 0.00042 0.02 0.0022	0.02 0.012 0.12 0.03	0.299 0.088 0.511 0.2835	- - -	Depleted MORB mantle (DMM) Salters and Stracke (2004) - 2 GPa - DMM Primitive mantle (PM)	0.045 0.060 0.065	0.015 0.020 0.021	0.111 0.137 0.141	0.047 0.061 0.065	3.00 3.08 3.16	2.40 2.26 2.18	0.80 0.73 0.69	Fig. 3c	
Salters and Stracke (2004) - 3 GPa	Sm Nd Lu Hf	0.0011 0.00042 0.02 0.0011	0.02 0.012 0.12 0.024	0.1509 0.0884 0.276 0.14	0.23 0.064 7 0.4	Salters and Stracke (2004) - 3 GPa - DMM PM including garnet	0.065 0.041	0.034 0.022	0.464 0.300	0.070 0.044	1.89 1.88	6.62 6.74	3.51 3.59	Fig. 3d	
Kelemen et al. (2003)	Sm Nd Lu Hf	0.0007 0.00007 0.03 0.004	0.02 0.009 0.12 0.04	0.291 0.1873 0.433 0.256	0.217 0.057 9 0.5	Depleted MORB mantle (DMM) Primitive mantle (PM) PM including garnet Salters and Stracke (2004) - 2 GPa - DMM	0.044 0.063 0.067 0.059	0.027 0.040 0.039 0.036	0.107 0.131 0.395 0.129	0.047 0.063 0.075 0.060	1.63 1.60 1.69 1.61	2.29 2.09 5.30 2.15	1.40 1.31 3.13 1.34	Fig. 3b	
Average Max Min							0.055 0.067 0.041	0.028 0.040 0.015	0.204 0.464 0.107	0.057 0.075 0.035	2.098 3.157 1.452	3.545 6.743 2.095	1.886 3.587 0.690		

Mineral modes											
	Olivine	Opx	Срх	Garnet							
Depleted MORB mantle (DMM)	0.57	0.28	0.13	0							
Salters and Stracke (2004) - 2 GPa - DMM	0.53	0.29	0.18	0							
Salters and Stracke (2004) - 3 GPa - DMM	0.53	0.08	0.34	0.05							
Primitive mantle (PM)	0.57	0.23	0.20	0							
PM including garnet	0.56	0.22	0.19	0.03							

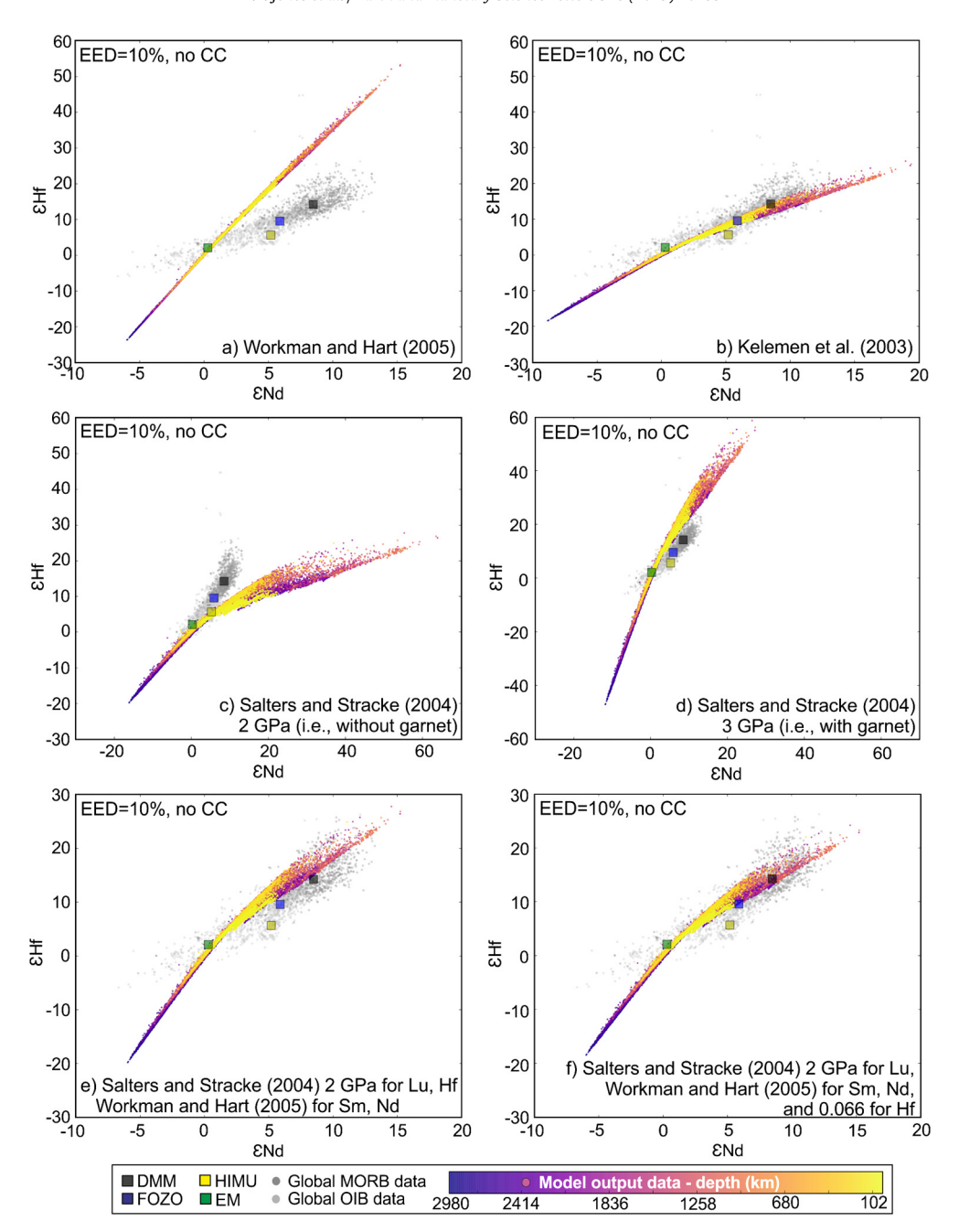


Fig. 3. Plots of $ε_{Nd}$ versus $ε_{Hf}$ comparing the model chemistry (after 4.55 Byr with various bulk D values) to the global MORB-OIB dataset; a) bulk D values of Workman and Hart (2005); b) Kd values from Kelemen et al. (2003) combined with the mineral abundances for DMM at 2 GPa from Salters and Stracke (2004); c) bulk D values from Salters and Stracke (2004) for DMM at 2 GPa (i.e., without garnet); d) bulk D values from Salters and Stracke (2004) for DMM at 3 GPa (i.e., with garnet); e) bulk D values from Workman and Hart (2005) for Sm and Nd, and from Salters and Stracke (2004) for Lu and Hf (DMM at 2 GPa); and f) bulk D values from Workman and Hart (2005) for Sm and Nd, bulk D value from Salters and Stracke (2004) for Lu (DMM at 2 GPa), and an assumed bulk D value of 0.066 for Hf. The formation of continental crust (CC) is not implemented in these models and all models use 10% excess eclogite density (EED = 10%) as this always produces the most extreme range in values. Note the changing axis values and that the model data is coloured according to depth.

Although the simple production, recycling, and storing of OC in the model produces a good fit between the model data and the global data array (e.g., Fig. 4b), it fails to reproduce the Hf and Nd isotope compositions of the UM. Even the most extreme EED model (EED = 10%) has average UM $\varepsilon_{\rm Hf}$ and $\varepsilon_{\rm Nd}$ compositions of only +6.3 and +3.0 respectively (Fig. 4c and f).

3.4. The production and recycling of continental crust

In the third stage of modelling we tested the effects of producing and recycling of continental crust (CC). The retention coefficients implemented change depending on the EED, partition

coefficients, and whether CC is recycled (Table S1). Here, we focus on the 10% EED model (Fig. 6), as it produces UM compositions that are closest to the observed values (Section 3.3). The results from the production and recycling of CC in the EED = 0% and EED = 7% models are shown in Supplementary Figs. S2 and S3.

The generation of CC in the model (1 \times CC_{pd} extracted) produces a slightly more restricted and positive data array with a broader spread in Hf isotope compositions (Fig. 6a compared to 4c). The composition of the lower mantle does not evolve to such unradiogenic Hf isotope compositions, with a maximum final $\varepsilon_{\rm Hf}$ of -10.2 compared to -13.6 without CC extraction (Fig. 6b compared to 4f). This is due to the preferential extraction of incompati-

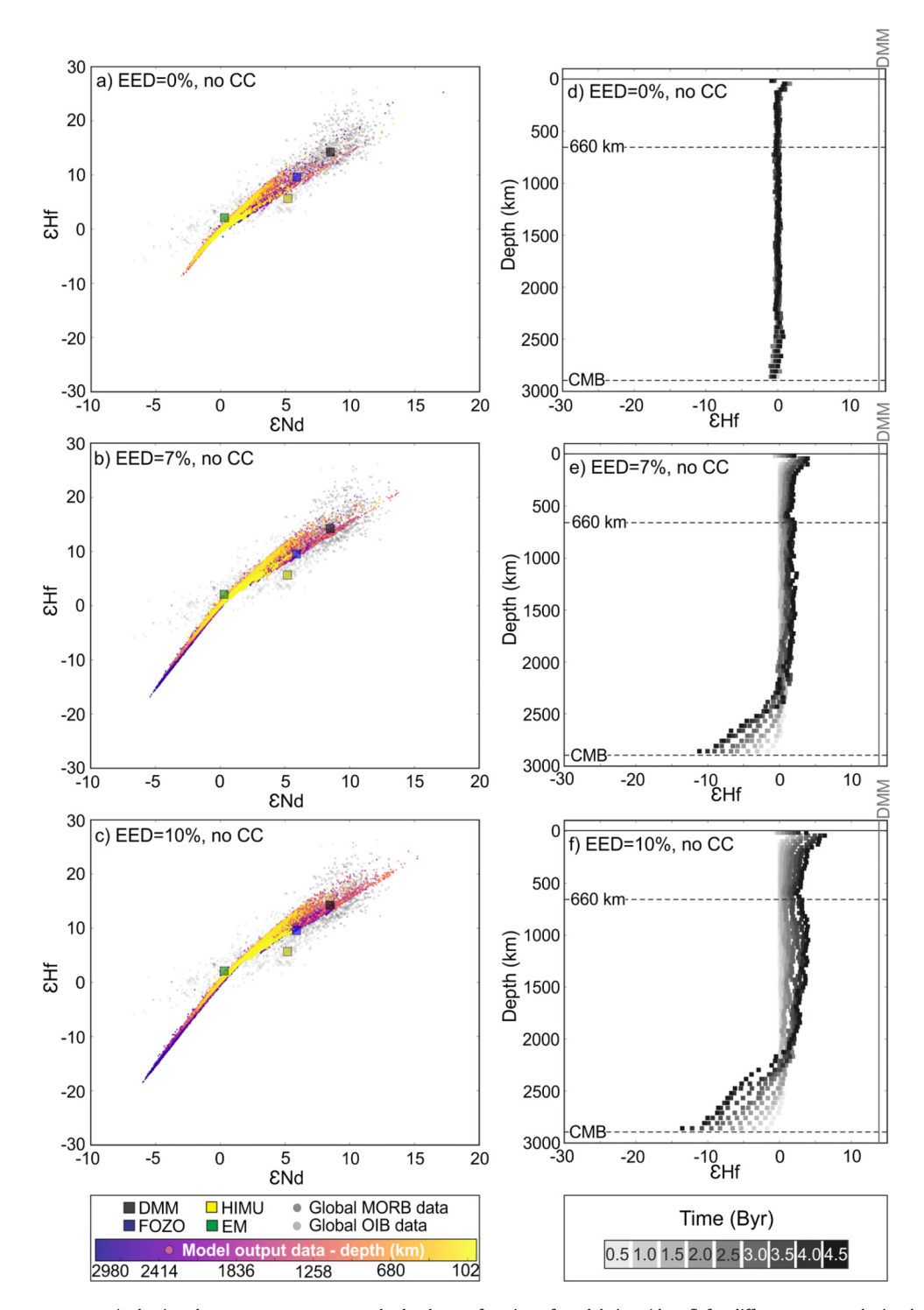


Fig. 4. Plots of final ε_{Nd} versus ε_{Hf} (a, b, c) and average ε_{Hf} versus mantle depth as a function of model time (d, e, f) for different excess eclogite densities (EED); a and d show the results for the neutral case (EED = 0%); b and e for 7% EED; and, c and f for 10% EED. These models assume the bulk D values from Workman and Hart (2005) for Sm and Nd, the bulk D value from Salters and Stracke (2004) for Lu (DMM at 2 GPa), and a bulk D value of 0.066 for Hf. No continental crust (CC) was produced in these models.

ble TE into the CC, forming a competing, unradiogenic and negative $\varepsilon_{\rm Hf}$ and $\varepsilon_{\rm Nd}$ reservoir over time. As a result of this depletion, the rest of the mantle becomes more radiogenic in its Hf and Nd isotope composition (above 2500 km in Fig. 6b).

Dhuime et al. (2012) suggested that 100% of the present volume of the CC has been destroyed and recycled back into the mantle since 3 Ga. We simulated this by producing, over time, twice the present-day mass of the CC and recycling one mass back into

the mantle from 4.05 Ga ($2 \times CC_{pd}$ extracted, $1 \times CC_{pd}$ recycled). This generates more unradiogenic Hf and Nd isotope compositions in the lower mantle (below 660 km) and a Hf-Nd isotope array with a wider spread (Figs. 6d and e). As recycled CC is carried by the eclogite tracers, it follows their movement in the geodynamical model and is potentially stored in the deep mantle, producing greater compositional heterogeneity (Fig. 6d). Although recycling CC generates more heterogeneity, the average Hf and Nd isotope

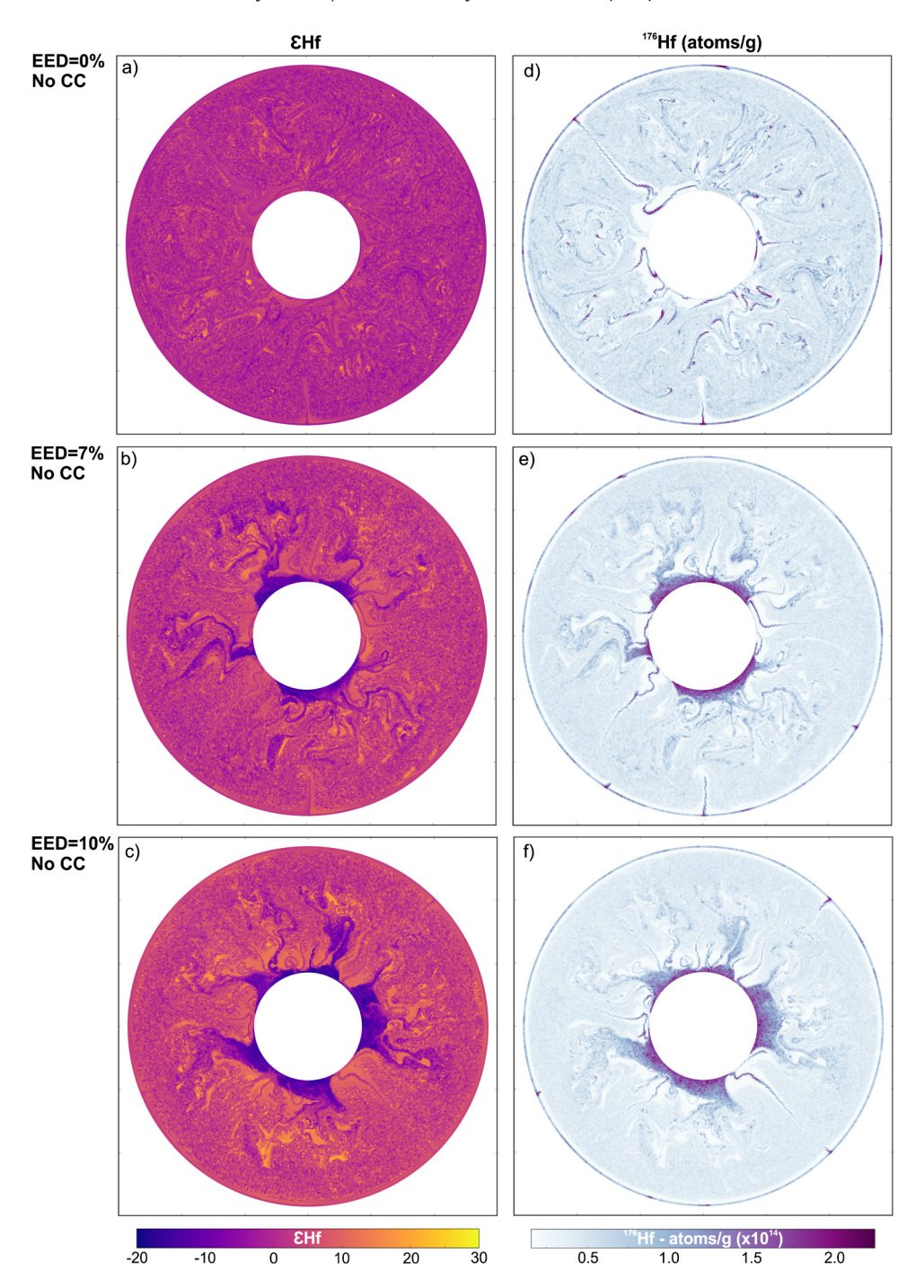


Fig. 5. Plots of final $\varepsilon_{\rm Hf}$ compositions and $^{176}{\rm Hf}$ concentrations (atoms/g) in the mantle after 4.55 Byr of mantle convection for different EED; a and d show the results for the neutral case (EED = 0%); b and e for 7% EED; and, c and f for 10% EED. Plots of final $\varepsilon_{\rm Nd}$ compositions and $^{143}{\rm Nd}$ concentrations (atoms/g) are shown in Supplementary Fig. S1.

compositions of the UM and at the CMB are similar to those produced without CC recycling (Figs. 6b and e). The recycling of CC produces more realistic Hf and Nd isotope compositions for the CC itself ($\varepsilon_{\rm Hf}$ and $\varepsilon_{\rm Nd}$ of -24 and -17, respectively) compared to the case without CC recycling (-33 and -22) (Figs. 6b and e). Since we keep the proportion of the CC recycled constant over model time, the CC extracted early in the model run that evolves to highly unradiogenic compositions is redistributed into the mantle via the eclogite tracers. This results in a CC that evolves to less extremely negative $\varepsilon_{\rm Hf}$ and $\varepsilon_{\rm Nd}$ compositions. Additionally, the growth of the CC without CC recycling is nearly linear (Fig. 6c). In contrast, when CC is recycled, the continental growth curve is initially steep and

then shallows implying that recycling becomes a more prevalent process over time (Fig. 6f). The latter qualitatively matches some of the proposed models for the growth of the CC primarily based on Hf isotopic compositions of zircons (e.g., Belousova et al., 2010; Dhuime et al., 2012).

The extraction and recycling of CC does generate more positive ϵ_{Hf} and ϵ_{Nd} compositions (+6 and +3) in the UM, compared to models without CC formation, but these still differ from the observed values. This suggests that the UM is not being sufficiently depleted in the daughter isotope relative to the parent isotope (i.e., D_{Sm}/D_{Nd} and D_{Lu}/D_{Hf} are too low) to develop more radiogenic Hf and Nd isotope compositions.

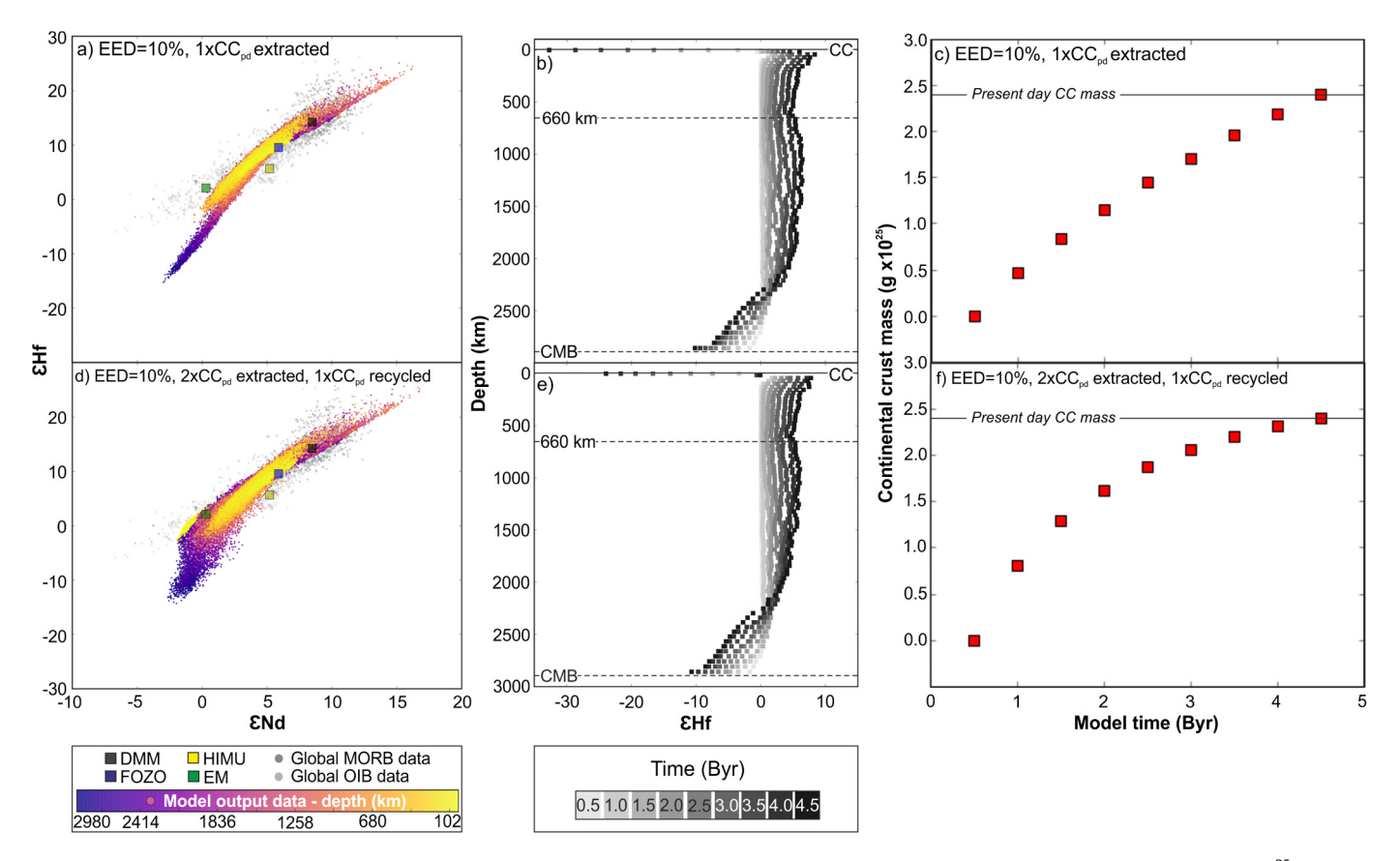


Fig. 6. Plots of final ε_{Nd} versus ε_{Hf} (a and d), and the time evolution of average ε_{Hf} versus mantle depth (b and e) and the mass of the continental crust (in 10^{25} g; frames c and f). The top row shows the results for the model in which one present-day mass of the continental crust (CC_{pd}) is formed from 0.5 Byr. The bottom row shows the results for the model where continental crust was both generated and recycled from 0.5 Byr (2 × CC_{pd} extracted, 1 × CC_{pd} recycled). Both models are for EED = 10% using the preferred partition coefficients detailed in section 3.2. The results for EED = 0% and EED = 7% can be found in Supplementary Figs. S2 and S3.

3.5. Re-assessing the prescribed partition coefficients

The models presented thus far fail to produce the observed radiogenic Hf and Nd isotope composition of the UM. In order to generate a complementary unradiogenic reservoir, the fractionation between the parent and daughter species could be changed to retain more Lu and Sm relative to Hf and Nd in the melting residue (harzburgite tracers). This would lead to more radiogenic Hf and Nd isotope compositions in the harzburgite and less radiogenic compositions in the eclogite. The spread and slope of the Hf-Nd isotope array is governed by $(D_{Lu}/D_{Hf})/(D_{Sm}/D_{Nd})$. The only satisfactory way we found to produce the Hf and Nd isotope compositions of the UM, and the slope of the Hf-Nd mantle array, was to adjust the bulk D values to increase the fractionation between the parent and daughter species. In the preferred model, the bulk D values used are Sm = 0.067, Nd = 0.015, Lu = 0.464 and Hf= 0.048 (Table 3), all of which are still within the range of the published values (Table 1). However, we recognise there is an immediate influence of the way we compute the melt fraction in the model, and therefore, our resulting preferred bulk D values are not necessarily representative of 'true' bulk D values.

To further ensure that the assigned bulk D values are not unrealistic, we applied batch melting to the average composition of the UM just below the depth of the melting zone (100–360 km) to check that the melt generated has a TE composition similar to MORB (Jenner and O'Neill, 2012, Supplementary Fig. S4). A good match is seen between the TE composition of batch melts produced from the average UM in the model with a melt fraction of between 10 and 15% and MORB composition with 9 wt.% MgO (Table 3). Increasing the EED depletes the UM in TE more strongly, due to increased storage of eclogite at the CMB. We also tested the

sensitivity of the model to different BSE compositions. For example, the BSE concentrations of Palme and O'Neill (2003) are higher for Lu, Hf, Sm and Nd compared to McDonough and Sun (1995). When these concentrations are utilised this also results in a more TE-enriched UM and, in this case, the composition of a MORB with 9 wt.% MgO is matched with a higher melt fraction (Table 3).

The results of our preferred model are presented in Fig. 7. To reproduce the Hf and Nd isotope compositions of the UM (Figs. 7b and c) the range of values throughout the mantle exceeds those exhibited in the Hf-Nd mantle array (Fig. 7a). Specifically, the values observed in the lower mantle spread to compositions not measured in OIB samples that are thought to be sourced from the lower mantle. The model lower mantle at the CMB has an average $\varepsilon_{\rm Hf}$ composition of -38 and $\varepsilon_{\rm Nd}$ of -14. The mantle above 2500 km depth has average compositions more radiogenic than CHUR (Bouvier et al., 2008), with the depleted UM showing the most positive $\varepsilon_{\rm Hf}$ and $\varepsilon_{\rm Nd}$ compositions of 12–18 and 7–10 respectively (Fig. 7). Without the production and recycling of CC (Fig. S5) the lower mantle evolves to similarly negative $\varepsilon_{\mathrm{Hf}}$ and $\varepsilon_{\mathrm{Nd}}$ values (-37 and -15), but the mantle above 2500 km depth evolves to less radiogenic compositions with the UM falling short of the DMM composition ($\varepsilon_{Hf} = 12$, $\varepsilon_{Nd} = 6$) (Table 3).

We note that the shape of the Hf and Nd isotope array produced by the preferred model is more curved than the measured array, but that the centre of the model array overlaps the mantle array and the model produces compositions that match the DMM, FOZO, and EM mantle endmembers (Fig. 7). The increased curvature is primarily caused by the trajectory in the model array that has higher $\varepsilon_{\rm Nd}$ than $\varepsilon_{\rm Hf}$ values. These compositions reflect the presence of ultra-depleted harzburgitic tracers, which have participated in more than one mantle melting event. In addition, as a

Table 2Constant parameters in the geochemical model.

Fixed parameters			Reference
Age of the Earth (yr)		4.55×10^{9}	
Mass of the mantle (g)		4.04×10^{27}	
Mass of the continental crust (g)		2.40×10^{25}	
Concentration of stable isotope species in the mantle (atoms/g)	¹⁴⁴ Nd ¹⁷⁷ Hf	$\begin{array}{c} 1.242 \times 10^{15} \\ 1.776 \times 10^{14} \end{array}$	Calculated using BSE values of McDonough and Sun (1995) and isotope abundances of Meija et al. (2016)
Decay constants (yr^{-1})	¹⁴⁷ Sm	6.53915×10^{-12}	Begemann et al. (2001)
	¹⁷⁶ Lu	1.867×10^{-11}	Söderlund et al. (2004)
CHUR values	¹⁴⁷ Sm/ ¹⁴⁴ Nd	0.1960	Bouvier et al. (2008)
	¹⁴³ Nd/ ¹⁴⁴ Nd ¹⁷⁶ Lu/ ¹⁷⁷ Hf ¹⁷⁶ Hf/ ¹⁷⁷ Hf	0.512630 0.0336 0.282785	
Concentration of isotope species in the continental crust (atoms/g)	¹⁴⁷ Sm ¹⁴⁴ Nd ¹⁷⁶ Lu ¹⁷⁷ Hf	5.623×10^{40} 4.769×10^{41} 6.441×10^{38} 5.573×10^{40}	Calculated using continental crust composition of Rudnick and Gao (2014) and isotope abundances of Meija et al. (2016)

Table 3

Model results for different EED, BSE values, bulk D values, melt fractions, timing of crust production, and assumptions on production and recycling of continental crust. Here the upper mantle is considered to be at depths in the model of between 100 (i.e., below the melting zone) and 360 km. The Hf and Nd concentrations (ppm) of an upper mantle melt are calculated by applying batch melting equations to the average composition of the upper mantle, with varying melt fractions. These calculated concentrations are compared to those reported by Jenner and O'Neill (2012) for a MORB with 9 wt.% MgO (1.3 ppm Hf and 5.5 ppm Nd, Fig. S4); the closest calculated values are underlined. The preferred model (Fig. 7) is highlighted in bold. An extended table is given in the Supplementary Data Tables.

Geochemical model inputs								Geochemical model outputs				Batch melting the upper mantle						Associated
EED model	Key parameter	BSE values	Bulk D values				Continental	Average upper mantle		Element	Average	Varying melt fraction					figure	
	change		Sm	Nd	Lu	Hf	crust	Epsilon Hf	Epsilon Nd		upper mantle (ppm)	0.01	0.05	0.1	0.125	0.15	0.2	
EED010	Adjusted bulk D values	McDonough and Sun (1995)	0.0450	0.0310	0.137	0.066	None	4.0	1.6	Hf Nd	0.23 0.97	3.09 23.95	2.07 12.26	1.46 7.62	1.27 6.41	1.13 5.53	0.92 4.33	Fig. 3f
EED010	Adjusted bulk D values	McDonough and Sun	0.0670	0.0150	0.464	0.048	Production and	14.4	8.0	Hf	0.22	3.75	2.26	<u>1.51</u>	1.29	1.13	0.91	Fig. 7
		(1995)					recycling			Nd	0.88	35.49	13.73	7.77	6.38	5.42	4.16	
EED010	No continental crust	McDonough and Sun	0.0670	0.0150	0.464	0.048	None	12.0	6.0	Hf	0.23	3.95	2.38	1.59	1.36	1.19	0.95	Fig. S5
		(1995)								Nd	0.94	37.89	14.66	8.30	6.82	5.79	4.44	
EED007	Lower EED (7%)	McDonough and Sun	0.0670	0.0150	0.464	0.048	Production and	9.0	5.3	Hf	0.23	3.95	2.38	1.59	1.36	1.19	0.95	Fig. S6
		(1995)					recycling			Nd	0.95	38.09	14.73	8.34	6.85	5.82	4.47	
EED010	Late stage mantle	McDonough and Sun	0.0670	0.0150	0.464	0.048	Production and	10.6	6.3	Hf	0.23	3.92	2.36	1.57	1.35	1.18	0.94	Fig. S8
	depletion (after 0.75 Byr)	(1995)					recycling			Nd	0.93	37.37	14.45	8.18	6.72	5.71	4.38	
EED010	Different BSE starting	Palme and O'Neill	0.0670	0.0150	0.464	0.048	Production and	14.2	7.8	Hf	0.23	3.99	2.40	1.60	1.37	1.20	0.96	_
	values	(2003)					recycling			Nd	0.94	37.81	14.62	8.28	6.80	5.77	4.43	
EED010	25% increase in melt	McDonough and Sun	0.0670	0.0150	0.464	0.048	Production and	14.5	7.1	Hf	0.21	3.69	2.22	1.48	1.27	1.11	0.89	Fig. S9
	fraction (F)	(1995)					recycling			Nd	0.87	35.19	13.61	7.70	6.33	5.37	4.12	-

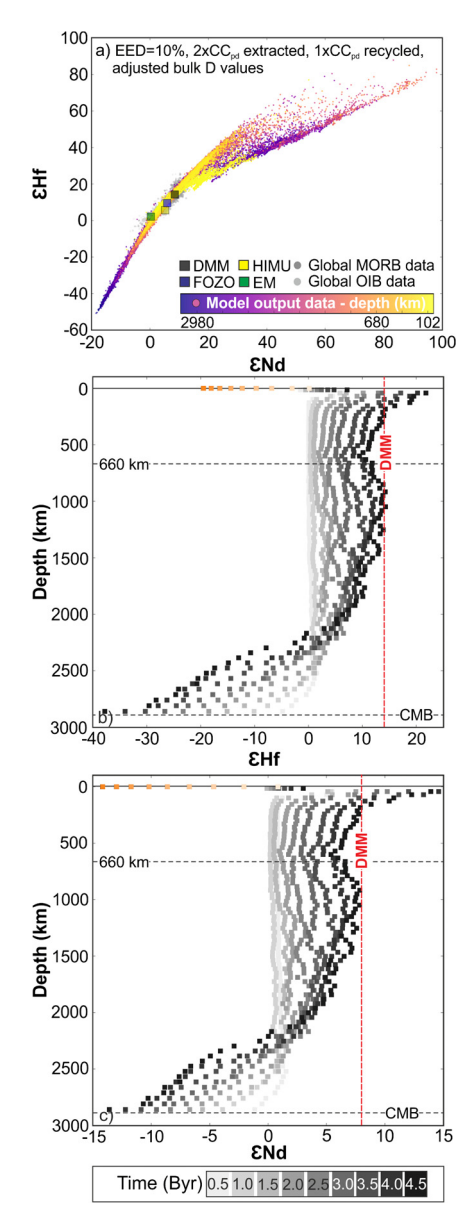


Fig. 7. Plots of final ε_{Nd} versus ε_{Hf} (a), average ε_{Hf} versus mantle depth (b), and average ε_{Nd} versus mantle depth (c) for the preferred model (EED = 10%, continental crust produced and recycled, and bulk D values set to maximum values (Sm = 0.0670, Nd = 0.0220, Lu = 0.464 and Hf = 0.075) to achieve upper mantle ε_{Hf} and ε_{Nd} compositions and reasonable trace element compositions (Table 3)). Results without continental crust formation and recycling and 7% EED are shown in Figs. S5 and S6

result of the adjustment of the partition coefficients, the Hf-Nd array loses the 'cone-like' shape shown in Fig. 6d. This is due to the adjusted partition coefficients extending the values in the array to more extreme values, which reduces the apparent effect of CC recycling.

4. Discussion

4.1. Sensitivity to partition coefficients

The results of the geodynamical-geochemical model are highly sensitive to the prescribed bulk D values (much more so than to melt fraction, shown in Table 3 and Fig. S9). Parent and daughter species have different compatibilities in different mantle minerals, and therefore the Lu/Hf and Sm/Nd of the melt is controlled by the minerals present in the source. Lu has a much higher compat-

ibility in garnet (and somewhat higher in clinopyroxene) than Hf (Table 1), meaning the presence of even a small amount of garnet (typically stable at P>1 GPa) in the melt source region would result in a lower amount of Lu, relative to Hf being partitioned into the OC. Similarly, Sm has a higher compatibility in garnet and clinopyroxene compared to Nd.

Present day MORBs are thought to be primarily produced from melting in the spinel stability field (<60 km depth) and there is likely to be little garnet present. However, the abundance of certain mineral phases in the melt source region, and which stability field (garnet versus spinel and plagioclase) melting occurred in, has likely changed over the course of Earth history. The Archean mantle is widely considered to be hotter than the modern mantle (e.g., Herzberg et al., 2010 and references therein), which would have resulted in a higher degree of partial melting and the production of a thicker, warmer, and more buoyant OC (e.g., Sleep and Windley, 1982; Bickle, 1986). In our preferred model the partition coefficients were adjusted to increase the fractionation between the parent (Lu and Sm) and daughter (Hf and Nd) species. This could be accounted for by the presence of residual garnet in the melt source region in the early Earth when melting may have occurred at deeper levels, due to the thickness of the overlying crust. Salters and Hart (1989) also suggested that the Lu-Hf and Sm-Nd systematics of MORBs requires garnet to be a residual phase in melt genesis, and proposed a model in which melting starts in the garnet stability field and then continues at shallower levels. Hirschmann and Stolper (1996), alternatively, propose that the combination of spinel peridotite with 3-6% pyroxenite, with >20% modal garnet, could also account for the Lu-Hf and Sm-Nd compositions of most MORB. Our model supports an increased role for garnet and, overall, suggests that elemental partition coefficients, combined with present-day MORB source mineral abundances and melt fractions, may not be appropriate for the entirety of Earth evolution.

The adjusted partition coefficients in the preferred model produce a range of Hf and Nd isotope compositions not observed in the MORB-OIB mantle array (Fig. 7a). However, extremely high $\varepsilon_{\rm Hf}$ and ε_{Nd} values (60 and 21 respectively) have been reported for abyssal peridotites that represent residual mantle (Stracke et al., 2011). These compositions have been attributed to ancient mantle depletion, with the comparatively unradiogenic Nd isotope compositions reflecting higher susceptibility to resetting by melt-rock interaction of Sm-Nd compared to Lu-Hf. A number of studies have also suggested that the mantle is more heterogeneous in composition and contains more extreme isotopic compositions than have been measured in MORB and OIB to date (e.g., Bizimis et al., 2007; Liu et al., 2008; Stracke et al., 2011). This is consistent with the model results presented here. The extreme isotopic compositions contained in portions of the residual mantle are unlikely to be reflected in MORB and OIB compositions, as these domains are refractory and thus contribute little to the genesis of magmas, and their compositions are easily overprinted by melting of more TE enriched, fertile portions of the mantle.

A recent study has reported chondritic Hf isotopic compositions of Eoarchean zircons and interpreted this as evidence that there was no early, planet-scale depletion of the mantle in the Hf isotope record prior to 3.8 Ga (Fisher and Vervoort, 2018). We tested this scenario of late stage mantle depletion and found negligible impact on the geochemical evolution (Table 3, Fig. S8). The $\varepsilon_{\rm Hf}$ and $\varepsilon_{\rm Nd}$ compositions obtained for the upper mantle were slightly lower than observed, but a match could be made by further adjustment of the model partition coefficients.

4.2. Variations with depth and the development of OIB endmember compositions

The least radiogenic Hf and Nd isotope compositions in all results are found in eclogite that experienced melting early and was subducted and stored in the deep mantle (Figs. 3–7). Increasing EED results in increasingly unradiogenic Hf and Nd isotope compositions (Fig. 4), as more eclogite is retained near the CMB. The negative $\varepsilon_{\rm Hf}$ and $\varepsilon_{\rm Nd}$ region of the mantle array is occupied by the enriched mantle compositions such as those obtained for EMI and EMII OIBs. These EM compositions have been linked with the recycling of sediments, delaminated lower CC, or metasomatised subcontinental lithosphere (e.g., Zindler and Hart, 1986; Weaver, 1991; Chauvel et al., 1992; Tatsumoto et al., 1992; Eisele et al., 2002; Willbold and Stracke, 2006, 2010). The results presented here suggest that the incorporation of OC recycled into the source of OIBs could partly account for the EM compositions.

The results also support, in part, the conclusions of earlier combined geodynamical-geochemical models (e.g., Christensen and Hofmann, 1994; Davies, 2002; Xie and Tackley, 2004; Brandenburg et al., 2008), which suggested that the pooling of dense OC at the CMB plays a fundamental role in developing MORB and OIB compositions. These previous studies, however, tended to focus on the U-Th-Pb isotope systems and the development of HIMU mantle compositions. In this study we do not produce HIMU and extreme EMII Hf and Nd isotope compositions, suggesting that a geochemical component, such as recycled oceanic sediments, is missing. Chauvel et al. (2008) suggested that the Hf-Nd mantle array cannot be produced from the recycling of basaltic OC alone and invoked the need for recycling of both OC and sediments (over 3 Byr) into the source of OIBs to produce MORB-OIB compositions. In contrast, our model results show that a large proportion of the Hf-Nd mantle array can be produced by the recycling of OC alone (Fig. S5). Producing and recycling CC produces a wider spread in the Hf-Nd isotope array (Fig. 7), but recycling oceanic sediments into the mantle, which have a shallower Hf-Nd isotope array (Chauvel et al., 2008) (not modelled here), may be required to generate the full array (i.e., HIMU and extreme EMII compositions).

The extreme unradiogenic Hf and Nd isotope compositions produced in the lower mantle of the preferred model (Fig. 7a) are not observed in natural samples (Fig. 1). However, the isotopic compositions of the plumes rising in the model show a mixture of material being entrained into them with a range of compositions. Therefore, the less extreme compositions observed in OIB might reflect the mixing of recycled OC with more residual portions of the mantle, or mantle which has not undergone melting (e.g., Li et al., 2014), both of which would have more radiogenic Hf and Nd isotope compositions.

4.3. The growth of the continental crust

The formation of the CC in the model is rather simplistic and involves the extraction of incompatible TE from the eclogite tracers based on iteratively set retention coefficients. In the Earth this might reflect the formation of early CC from basaltic crust and subduction zone processes involving the dehydration and melting of down-going OC (e.g., Zegers and van Keken, 2001; Johnson et al., 2017; Gardiner et al., 2018). Although we set the retention coefficients arbitrarily, the values used in the preferred model (Table S1) generally mirror melt/mineral and fluid/mineral (Kessel et al., 2005) partitioning behaviour, with preferentially higher extraction of Hf and Nd into the CC compared to Lu and Sm.

Early geochemical models suggested that the formation of the CC is critical in developing the composition of the depleted mantle (e.g., Jacobsen and Wasserburg, 1979; Hofmann, 1988;

McCulloch and Bennett, 1994; Workman and Hart, 2005). In our preferred model the production and recycling of the CC has a limited effect in terms of matching the composition of the present-day UM, OIB endmembers, and the slope of the Hf-Nd mantle array (Fig. S5 shows the result without CC extraction and recycling). Instead, the formation, recycling, and critically the storage of OC near the CMB is found to be the more important process in determining the mantle and crustal Lu-Hf and Sm-Nd compositions. The mass of the OC produced in the model $(2.83 \times 10^{26} \text{ g, assuming})$ a constant rate of production for 4.55 Byr) is considerably greater than the mass of CC produced in the model (2.40×10^{25}) g, or 4.8×10^{25} g if one mass of the CC is recycled). Despite the higher enrichment of the CC in incompatible TE compared to the OC, the large mass of recycled OC stored in the deep mantle (with increased EED), which is also a longer-lived reservoir than the CC, provides a more effective mechanism of sequestering incompatible TE from the convecting mantle. This is supported by the TE composition of the UM produced in the model with and without the formation of CC. When CC is formed in the model, the UM is only marginally more depleted, and subsequently produces the composition of MORB (9 wt.% MgO) with a slightly lower melt fraction (Table 3).

The Hf and Nd isotope composition of the CC generated in the model more closely matches the average composition of the upper CC (Chauvel et al., 2014) when continental crust is recycled in the model (Fig. 6e). Without CC recycling the models develop average compositions that are too extreme due to the long residence time of the earliest formed CC (4.05 Ga) (Fig. 6b). Recycling continental crust into the mantle, which could occur through subduction of continental sediments, subduction erosion of continental crust, or delamination of thick continental crust, reduces the average Hf and Nd isotope compositions developed in the model CC. Thus our model lends support to the hypothesis that a volume of CC, equal to the present day volume of the continents, may have been recycled into the mantle over geological time (e.g., Dhuime et al., 2012). The final Hf and Nd isotope compositions obtained for the CC, even when continental recycling is implemented in the model, are still less radiogenic ($\varepsilon_{Hf}=-19.5$ and $\varepsilon_{Nd}=-14.2$) than the values proposed for the average upper CC ($\epsilon_{Hf} = -13.2 \pm 2.0$, and $\varepsilon_{\text{Nd}} = -10.3 \pm 1.2$ (Chauvel et al., 2014)). In order to generate the composition of the average upper continental crust, 200% of the present day mass of the CC would have to be recycled into the mantle. However, as no average $\varepsilon_{\mathrm{Hf}}$ and $\varepsilon_{\mathrm{Nd}}$ values have been proposed for the mid to lower CC, which may include a significant mass of older crust with lower $\varepsilon_{\mathrm{Hf}}$ and $\varepsilon_{\mathrm{Nd}}$, we consider the more negative $\varepsilon_{\mathrm{Hf}}$ and $\varepsilon_{\mathrm{Nd}}$ values obtained for the CC in our preferred model (Fig. 7b and c) to be suitably realistic.

Different workers have suggested different models for the growth of the continental crust, including early formation (Armstrong, 1981), episodic growth (e.g., Condie and Aster, 2010) and relatively late stage formation (after 2.5 Ga) (e.g., Allègre and Rousseau, 1984; for a review see Hawkesworth et al., 2019). Our results with CC recycling lead to a CC growth curve similar to those suggested by Belousova et al. (2010) and Dhuime et al. (2012), based on Hf isotopic compositions of zircons combined with U-Pb ages (Fig. 6f). These growth curves suggest that a mass equivalent to 50–70% of the current CC mass was accumulated prior to 3 Ga. These studies go on to suggest that crustal recycling and reworking dominated over juvenile additions to the continental crust since at least the end of the Archean (2.5 Ga), possibly related to the onset of subduction-driven plate tectonics (Dhuime et al., 2012).

5. Conclusions

Our preferred model (based on excess eclogite density of 10%, with production and recycling of continental crust (CC), and ad-

justed bulk D values suggesting an increased role for residual garnet during mantle melting) reproduces the Hf and Nd isotope compositions of the upper mantle and continental crust. Negative $\varepsilon_{
m Hf}$ and $\varepsilon_{\mathrm{Nd}}$ are consistently observed in the lower mantle in all model results and are caused by subducted and deeply accumulated oceanic crust. These compositions are similar to OIB enriched mantle endmembers (EMI and EMII), suggesting they are derived from the deep mantle. To generate the trace element depleted and radiogenic Hf and Nd isotope compositions of the upper mantle, the Earth must have a mechanism of generating and preserving a trace element (TE) enriched and unradiogenic Hf and Nd isotope reservoir somewhere in the mantle or crust. Previous geochemical studies have suggested the extraction of the continental crust is a critical process in generating the TE and isotopic composition of the upper mantle (e.g., Hofmann, 1988; McCulloch and Bennett, 1994; Workman and Hart, 2005). In contrast, we interpret the results of the combined geodynamical-geochemical modelling presented here to suggest that the extraction, subduction (and/or delamination), and critically the storage of oceanic crust in the lower mantle to be the key process driving the mantle-crust Lu-Hf and Sm-Nd systematics, with the formation and recycling of continental crust playing a lesser role. We suggest that the accumulation of recycled oceanic crust in the deep mantle provides a more effective mechanism of sequestering incompatible TE from the convecting mantle than the continental crust. This conclusion is reached based on the model reproducing both TE abundances and isotopic compositions of the upper mantle (DMM). The match to upper mantle compositions and the Hf-Nd mantle array is improved with CC production and recycling. The growth of the CC in the model is consistent with the continental growth curves based on Hf isotopic signatures obtained from zircon (Belousova et al., 2010; Dhuime et al., 2012), suggesting the growth of the continental crust is not a linear process through a simple steady-state extraction from the mantle. Including the recycling of oceanic sediments, which produce a shallower Hf and Nd isotope array (Chauvel et al., 2008), could extend the spread of the data generated by the model to the HIMU and extreme EMII compositions.

Acknowledgements

Rosemary Jones and Chris Ballentine acknowledge the support of the Natural Environment Research Council (NERC) Deep Mantle Volatiles consortium funding, NE/M000427/1. Peter van Keken and Jonathan Tucker acknowledge funding through the National Science Foundation CSEDI grant #1664642. We are grateful to Marianne Hasselhoff for assistance with Newton iteration coding. We extend our thanks to Catherine Chauvel and Andreas Stracke for their thorough and thoughtful comments, which have greatly improved the manuscript. Mike Bickle is thanked for editorial handling.

Appendix A. Supplementary material

Supplementary material related to this article can be found online at https://doi.org/10.1016/j.epsl.2019.04.015.

References

- Albarède, F., 1998. Time-dependent models of U-Th-He and K-Ar evolution and the layering of mantle convection. Chem. Geol. 145 (3–4), 413–429.
- Allègre, C.J., Lewin, E., 1995. Isotopic systems and stirring times of the Earth's mantle. Earth Planet. Sci. Lett. 136 (3–4), 629–646.
- Allègre, C.J., Rousseau, D., 1984. The growth of the continent through geological time studied by Nd isotope analysis of shales. Earth Planet. Sci. Lett. 67 (1), 19–34.
- Aoki, I., Takahashi, E., 2004. Density of MORB eclogite in the upper mantle. Phys. Earth Planet. Inter. 143–144, 129–143.
- Armstrong, R., 1981. Radiogenic isotopes: the case for crustal recycling on a nearsteady-state no-continental-growth Earth. Philos. Trans. R. Soc. Lond. A 301 (1461), 443–472.

- Begemann, F., Ludwig, K.R., Lugmair, G.W., Min, K., Nyquist, L.E., Patchett, P.J., Renne, P.R., Shih, C.Y., Villa, I.M., Walker, R.J., 2001. Call for an improved set of decay constants for geochronological use. Geochim. Cosmochim. Acta 65 (1), 111–121.
- Belousova, E., Kostitsyn, Y., Griffin, W.L., Begg, G.C., O'Reilly, S.Y., Pearson, N.J., 2010.
 The growth of the continental crust: constraints from zircon Hf-isotope data.
 Lithos 119 (3–4), 457–466.
- Bickle, M.J., 1986. Implications of melting for stabilisation of the lithosphere and heat loss in the Archaean. Earth Planet. Sci. Lett. 80 (3), 314–324.
- Bizimis, M., Griselin, M., Lassiter, J.C., Salters, V.J.M., Sen, G., 2007. Ancient recycled mantle lithosphere in the Hawaiian plume: osmium–hafnium isotopic evidence from peridotite mantle xenoliths. Earth Planet. Sci. Lett. 257 (1), 259–273.
- Bouvier, A., Vervoort, J.D., Patchett, P.J., 2008. The Lu–Hf and Sm–Nd isotopic composition of CHUR: constraints from unequilibrated chondrites and implications for the bulk composition of terrestrial planets. Earth Planet. Sci. Lett. 273 (1–2), 48–57
- Bowring, S.A., Williams, I.S., 1999. Priscoan (4.00–4.03 Ga) orthogneisses from northwestern Canada. Contrib. Mineral. Petrol. 134 (1), 3–16.
- Brandenburg, J., Hauri, E.H., van Keken, P.E., Ballentine, C.J., 2008. A multiple-system study of the geochemical evolution of the mantle with force-balanced plates and thermochemical effects. Earth Planet. Sci. Lett. 276 (1–2), 1–13.
- Brandenburg, J., van Keken, P., 2007. Deep storage of oceanic crust in a vigorously convecting mantle. J. Geophys. Res. 112 (B6), B06403.
- Chauvel, C., Blichert-Toft, J., 2001. A hafnium isotope and trace element perspective on melting of the depleted mantle. Earth Planet. Sci. Lett. 190 (3), 137–151.
- Chauvel, C., Garçon, M., Bureau, S., Besnault, A., Jahn, B.-m., Ding, Z., 2014. Constraints from loess on the Hf-Nd isotopic composition of the upper continental crust. Earth Planet. Sci. Lett. 388, 48–58.
- Chauvel, C., Hofmann, A.W., Vidal, P., 1992. HIMU-EM: the French Polynesian connection. Farth Planet. Sci. Lett. 110 (1), 99-119.
- Chauvel, C., Lewin, E., Carpentier, M., Arndt, N.T., Marini, J.-C., 2008. Role of recycled oceanic basalt and sediment in generating the Hf-Nd mantle array. Nat. Geosci. 1 (1), 64-67.
- Christensen, U.R., Hofmann, A.W., 1994. Segregation of subducted oceanic crust in the convecting mantle. J. Geophys. Res., Solid Earth 99 (B10), 19867–19884.
- Coltice, N., Ricard, Y., 1999. Geochemical observations and one layer mantle convection. Earth Planet. Sci. Lett. 174 (1), 125–137.
- Condie, K.C., Aster, R.C., 2010. Episodic zircon age spectra of orogenic granitoids: the supercontinent connection and continental growth. Precambrian Res. 180 (3–4), 227–236
- Condie, K.C., Bickford, M., Aster, R.C., Belousova, E., Scholl, D.W., 2011. Episodic zircon ages, Hf isotopic composition, and the preservation rate of continental crust. Geol. Soc. Am. Bull. 123 (5–6), 951–957.
- Davies, G.F., 2002. Stirring geochemistry in mantle convection models with stiff plates and slabs. Geochim. Cosmochim. Acta 66 (17), 3125–3142.
- Dhuime, B., Hawkesworth, C.J., Cawood, P.A., Storey, C.D., 2012. A change in the geodynamics of continental growth 3 billion years ago. Science 335 (6074), 1334–1336.
- Eisele, J., Sharma, M., Galer, S.J.G., Blichert-Toft, J., Devey, C.W., Hofmann, A.W., 2002. The role of sediment recycling in EM-1 inferred from Os, Pb, Hf, Nd, Sr isotope and trace element systematics of the Pitcairn hotspot. Earth Planet. Sci. Lett. 196 (3–4), 197–212.
- Elliott, T., Zindler, A., Bourdon, B., 1999. Exploring the kappa conundrum: the role of recycling in the lead isotope evolution of the mantle. Earth Planet. Sci. Lett. 169 (1), 129–145.
- Fisher, C.M., Vervoort, J.D., 2018. Using the magmatic record to constrain the growth of continental crust—the Eoarchean zircon Hf record of Greenland. Earth Planet. Sci. Lett. 488. 79–91.
- Fisher, C.M., Vervoort, J.D., DuFrane, S.A., 2014. Accurate Hf isotope determinations of complex zircons using the "laser ablation split stream" method. Geochem. Geophys. Geosyst. 15 (1), 121–139.
- Gardiner, N.J., Johnson, T.E., Kirkland, C.L., Smithies, R.H., 2018. Melting controls on the lutetium-hafnium evolution of Archaean crust. Precambrian Res. 305, 479–488.
- Hanyu, T., Kawabata, H., Tatsumi, Y., Kimura, J.-I., Hyodo, H., Sato, K., Miyazaki, T., Chang, Q., Hirahara, Y., Takahashi, T., Senda, R., Nakai, S.i., 2014. Isotope evolution in the HIMU reservoir beneath St. Helena: implications for the mantle recycling of U and Th. Geochim. Cosmochim. Acta 143, 232–252.
- Hawkesworth, C., Cawood, P.A., Dhuime, B., 2019. Rates of generation and growth of the continental crust. Geosci. Front. 10 (1), 165–173.
- Hawkesworth, C.J., Kemp, A.I.S., 2006. Using hafnium and oxygen isotopes in zircons to unravel the record of crustal evolution. Chem. Geol. 226 (3), 144–162.
- Herzberg, C., Condie, K., Korenaga, J., 2010. Thermal history of the Earth and its petrological expression. Earth Planet. Sci. Lett. 292 (1), 79–88.
- Hirose, K., Takafuji, N., Sata, N., Ohishi, Y., 2005. Phase transition and density of subducted MORB crust in the lower mantle. Earth Planet. Sci. Lett. 237 (1), 239–251.
- Hirschmann, M.M., Stolper, E.M., 1996. A possible role for garnet pyroxenite in the origin of the "garnet signature" in MORB. Contrib. Mineral. Petrol. 124 (2), 185–208.
- Hofmann, A.W., 1988. Chemical differentiation of the Earth: the relationship between mantle, continental crust, and oceanic crust. Earth Planet. Sci. Lett. 90 (3), 297–314.

- Hofmann, A.W., 1997. Mantle geochemistry: the message from oceanic volcanism. Nature 385 (6613), 219–229.
- Irifune, T., 1987. An experimental investigation of the pyroxene-garnet transformation in a pyrolite composition and its bearing on the constitution of the mantle. Phys. Earth Planet, Inter. 45 (4), 324–336.
- Jacobsen, S.B., Wasserburg, G., 1979. The mean age of mantle and crustal reservoirs. J. Geophys. Res., Solid Earth 84 (B13), 7411–7427.
- Jenner, F.E., O'Neill, H.S.C., 2012. Analysis of 60 elements in 616 ocean floor basaltic glasses. Geochem. Geophys. Geosyst. 13 (1), Q02005.
- Johnson, T.E., Brown, M., Gardiner, N.J., Kirkland, C.L., Smithies, R.H., 2017. Earth's first stable continents did not form by subduction. Nature 543, 239–242.
- Jones, R.E., Kirstein, L.A., Kasemann, S.A., Dhuime, B., Elliott, T., Litvak, V.D., Alonso, R., Hinton, R., 2015. Geodynamic controls on the contamination of Cenozoic arc magmas in the southern Central Andes: insights from the O and Hf isotopic composition of zircon. Geochim. Cosmochim. Acta 164, 386–402.
- Kelemen, P.B., Yogodzinski, G.M., Scholl, D.W., 2003. Along-strike variation in the Aleutian island arc: genesis of high Mg# andesite and implications for continental crust. In: Eiler, J. (Ed.), Inside the Subduction Factory. American Geophysical Union, Washington DC, pp. 223–276.
- Kellogg, J.B., Jacobsen, S.B., O'Connell, R.J., 2007. Modeling lead isotopic heterogeneity in mid-ocean ridge basalts. Earth Planet. Sci. Lett. 262 (3–4), 328–342.
- Kessel, R., Schmidt, M.W., Ulmer, P., Pettke, T., 2005. Trace element signature of subduction-zone fluids, melts and supercritical liquids at 120–180 km depth. Nature 437, 724–727.
- Kesson, S.E., Fitz Gerald, J.D., Shelley, J.M.G., 1994. Mineral chemistry and density of subducted basaltic crust at lower-mantle pressures. Nature 372, 767–769.
- Kinny, P.D., Maas, R., 2003. Lu-Hf and Sm-Nd isotope systems in zircon. Rev. Mineral. Geochem. 53 (1), 327-341.
- Kogiso, T., Tatsumi, Y., Nakano, S., 1997. Trace element transport during dehydration processes in the subducted oceanic crust: 1. Experiments and implications for the origin of ocean island basalts. Earth Planet, Sci. Lett. 148 (1–2), 193–205.
- Kumari, S., Paul, D., Stracke, A., 2016. Open system models of isotopic evolution in Earth's silicate reservoirs: implications for crustal growth and mantle heterogeneity. Geochim. Cosmochim. Acta 195, 142–157.
- Li, M., McNamara, A.K., Garnero, E.J., 2014. Chemical complexity of hotspots caused by cycling oceanic crust through mantle reservoirs. Nat. Geosci. 7, 366–370.
- Liu, C.-Z., Snow, J.E., Hellebrand, E., Brügmann, G., von der Handt, A., Büchl, A., Hofmann, A.W., 2008. Ancient, highly heterogeneous mantle beneath Gakkel ridge, Arctic Ocean. Nature 452, 311–316.
- McCulloch, M.T., Bennett, V.C., 1994. Progressive growth of the Earth's continental crust and depleted mantle: geochemical constraints. Geochim. Cosmochim. Acta 58 (21), 4717–4738.
- McDonough, W.F., Sun, S.-S., 1995. The composition of the Earth. Chem. Geol. 120 (3-4), 223-253.
- McKenzie, D., Bickle, M., 1988. The volume and composition of melt generated by extension of the lithosphere. J. Petrol. 29 (3), 625–679.
- Meija, J., Coplen, T.B., Berglund, M., Brand, W.A., De Bièvre, P., Gröning, M., Holden, N.E., Irrgeher, J., Loss, R.D., Walczyk, T., Prohaska, T., 2016. Isotopic compositions of the elements 2013 (IUPAC technical report). Pure Appl. Chem. 88 (3), 293–306.
- Ono, S., Ohishi, Y., Isshiki, M., Watanuki, T., 2005. In situ X-ray observations of phase assemblages in peridotite and basalt compositions at lower mantle conditions: implications for density of subducted oceanic plate. J. Geophys. Res., Solid Earth 110 (B2), B02208.
- Palme, H., O'Neill, H.S.C., 2003. Cosmochemical estimates of mantle composition. In: Carlson, R.W. (Ed.), The Mantle and Core, vol. 2. In: Holland, H.D., Turekian, K.K. (Eds.), Treatise on Geochemistry, vol. 1. Elsevier, Oxford, pp. 1–38.
- Peucker-Ehrenbrink, B., Hofmann, A.W., Hart, S.R., 1994. Hydrothermal lead transfer from mantle to continental crust: the role of metalliferous sediments. Earth Planet. Sci. Lett. 125 (1), 129–142.
- Ricolleau, A., Perrillat, J.P., Fiquet, G., Daniel, I., Matas, J., Addad, A., Menguy, N., Cardon, H., Mezouar, M., Guignot, N., 2010. Phase relations and equation of state of a natural MORB: implications for the density profile of subducted oceanic crust in the Earth's lower mantle. J. Geophys. Res., Solid Earth 115 (B8), B08202.
- Ringwood, A.E., 1990. Slab-mantle interactions: 3. Petrogenesis of intraplate magmas and structure of the upper mantle. Chem. Geol. 82, 187–207.
- Ritsema, J., Deuss, A., Van Heijst, H., Woodhouse, J., 2011. S40RTS: a degree-40 shear-velocity model for the mantle from new Rayleigh wave dispersion, teleseismic traveltime and normal-mode splitting function measurements. Geophys. J. Int. 184 (3), 1223–1236.

- Rudge, J.F., McKenzie, D., Haynes, P.H., 2005. A theoretical approach to understanding the isotopic heterogeneity of mid-ocean ridge basalt. Geochim. Cosmochim. Acta 69 (15), 3873–3887.
- Rudnick, R., Gao, S., 2014. Composition of the continental crust. In: Rudnick, R. (Ed.), The Crust, vol. 4. In: Holland, H.D., Turekian, K.K. (Eds.), Treatise on Geochemistry, vol. 2. Elsevier, Amsterdam, pp. 1–51.
- Salters, V.J., Stracke, A., 2004. Composition of the depleted mantle. Geochem. Geophys. Geosyst. 5 (5), Q05B07.
- Salters, V.J., White, W.M., 1998. Hf isotope constraints on mantle evolution. Chem. Geol. 145 (3), 447–460.
- Salters, V.J.M., Hart, S.R., 1989. The hafnium paradox and the role of garnet in the source of mid-ocean-ridge basalts. Nature 342, 420–422.
- Sleep, N.H., Windley, B.F., 1982. Archean plate tectonics: constraints and inferences. J. Geol. 90 (4), 363–379.
- Söderlund, U., Patchett, P.J., Vervoort, J.D., Isachsen, C.E., 2004. The ¹⁷⁶Lu decay constant determined by Lu–Hf and U–Pb isotope systematics of Precambrian mafic intrusions. Earth Planet. Sci. Lett. 219 (3–4), 311–324.
- Spasojevic, S., Gurnis, M., Sutherland, R., 2010. Mantle upwellings above slab graveyards linked to the global geoid lows. Nat. Geosci. 3 (6), 435–438.
- Stracke, A., Hofmann, A.W., Hart, S.R., 2005. FOZO, HIMU, and the rest of the mantle zoo. Geochem. Geophys. Geosyst. 6 (5), Q05007.
- Stracke, A., Snow, J.E., Hellebrand, E., Von Der Handt, A., Bourdon, B., Birbaum, K., Günther, D., 2011. Abyssal peridotite Hf isotopes identify extreme mantle depletion. Earth Planet. Sci. Lett. 308 (3), 359–368.
- Tatsumoto, M., Basu, A.R., Wankang, H., Junwen, W., Guanghong, X., 1992. Sr, Nd, and Pb isotopes of ultramafic xenoliths in volcanic rocks of Eastern China: enriched components EMI and EMII in subcontinental lithosphere. Earth Planet. Sci. Lett. 113 (1), 107–128.
- Van der Hilst, R., Widiyantoro, S., Engdahl, E., 1997. Evidence for deep mantle circulation from global tomography. Nature 386 (6625), 578–584.
- van Keken, P., 2001. Cylindrical scaling for dynamical cooling models of the Earth. Phys. Earth Planet. Inter. 124 (1–2), 119–130.
- van Keken, P., 2013. Mantle mixing: processes and modelling. In: Karato, S. (Ed.), Physics and Chemistry of the Earth's Deep Interior. John Wiley & Sons, Chichester, pp. 351–371.
- Vervoort, J.D., Blichert-Toft, J., 1999. Evolution of the depleted mantle: Hf isotope evidence from juvenile rocks through time. Geochim. Cosmochim. Acta 63 (3), 533–556.
- Vervoort, J.D., Kemp, A.I., 2016. Clarifying the zircon Hf isotope record of crust—mantle evolution. Chem. Geol. 425, 65–75.
- Vervoort, J.D., Patchett, P.J., Blichert-Toft, J., Albarède, F., 1999. Relationships between Lu-Hf and Sm-Nd isotopic systems in the global sedimentary system. Earth Planet. Sci. Lett. 168 (1), 79–99.
- Vervoort, J.D., Plank, T., Prytulak, J., 2011. The Hf-Nd isotopic composition of marine sediments. Geochim. Cosmochim. Acta 75 (20), 5903-5926.
- Weaver, B.L., 1991. The origin of ocean island basalt end-member compositions: trace element and isotopic constraints. Earth Planet. Sci. Lett. 104 (2), 381–397.
- White, W.M., 1985. Sources of oceanic basalts: radiogenic isotopic evidence. Geology 13 (2), 115–118.
- White, W.M., 2015. Probing the Earth's deep interior through geochemistry. Geochem. Perspect. 4 (2), 95–251.
- White, W.M., Hofmann, A.W., 1982. Sr and Nd isotope geochemistry of oceanic basalts and mantle evolution. Nature 296, 821–825.
- Willbold, M., Stracke, A., 2006. Trace element composition of mantle end-members: implications for recycling of oceanic and upper and lower continental crust. Geochem. Geophys. Geosyst. 7 (4).
- Willbold, M., Stracke, A., 2010. Formation of enriched mantle components by recycling of upper and lower continental crust. Chem. Geol. 276 (3), 188–197.
- Workman, R.K., Hart, S.R., 2005. Major and trace element composition of the depleted MORB mantle (DMM). Earth Planet. Sci. Lett. 231 (1), 53–72.
- Xie, S., Tackley, P.J., 2004. Evolution of U-Pb and Sm-Nd systems in numerical models of mantle convection and plate tectonics. J. Geophys. Res. 109 (B11), B11204.
- Zegers, T.E., van Keken, P.E., 2001. Middle Archean continent formation by crustal delamination. Geology 29 (12), 1083–1086.
- Zindler, A., Hart, S., 1986. Chemical geodynamics. Rev. Earth Planet. Sci. 14 (1), 493–571.